CrystEngComm

Accepted Manuscript

ROYAL SOCIETY OF CHEMISTRY

www.rsc.org/crystengcomm

Cite this: DOI: 10.1039/c0xx00000x

www.rsc.org/xxxxxx

ARTICLE TYPE

Facile synthesis and visible photocatalytic activity of single-crystal $TiO_2/PbTiO_3$ heterostructured nanofiber composites

YiFeng Yu[a], Zhaohui Ren*[a], Ming Li[a], Siyu Gong [a], Simin Yin [a], Shan Jiang [a], Xiang Li [a], Xiao Wei [ab], Gang Xu [a], Ge Shen [a], Gaorong Han* [a]

Received (in XXX, XXX) Xth XXXXXXXXX 200X, Accepted Xth XXXXXXXXX 200X

DOI: 10.1039/b000000x

Single-crystal $TiO_2/PbTiO_3$ nanofiber composites were prepared by a simple hydrothermal synthesis and annealing treatment at 650 ℃, where pre-perovskite(PP) $PbTiO_3$(PTO) and tetrabutyl titanate (TBOT) were used as precursors. In the composites, anatase TiO_2 nanorods grew on the surface of tetragonal perovskite(TP) PTO nanofibers and formed sharp $TiO_2/PbTiO_3$ interfaces, leading to single-crystal heterostructures. The as-synthesized heterostructured nanofiber composites exhibited excellent photocatalytic activity for degradation of methylene blue (MB) under visible light irradiation (λ>400 nm). Especially, the composites $TiO_2/PbTiO_3$ TBOT: 0.4 mL showed the highest photocatalytic activity, and the degradation rate of MB was 0.02392 min^{-1}. Such photocatalytic activity of the heterostructured nanofiber composites was, supposedly, attributed to the large-scale formation of the sharp interfaces, which could be critical for the photogenerated charge carries separation and their transfer from the PTO phase to TiO_2. It is suggested that the obtained heterostructured nanofiber composites $TiO_2/PbTiO_3$ can be exploited as an alternative visible-light driven photocatalyst.

Introduction

Among many candidates for photocatalysts, titania has been extensively explored because of its excellent photocatalytic performance in organic pollutants degradation and water splitting to produce hydrogen.[1-5] However, the large band gap (3.0 eV for rutile and 3.2 eV for anatase)[6-8] of TiO_2 significantly hinders its applications in the visible light region, which consequently limits the efficient utilization of solar energy. In order to extend applications of TiO_2 to the visible light region, different approaches have been proposed and developed to tailor the crystal structure and band structures of TiO_2, including doping,[9-11] hydrogenation.[1,12] In addition, coupling of TiO_2 with other semiconductors capable of being sensitized by visible light, is often used,[13-14] where heterojunctions can promote charge separation through favorable band alignments, possibly leading to the reduction of recombination losses.[15] Up to now, many efforts have been devoted to fabricating TiO_2-based heterostructured composites, such as CdS/TiO_2,[16] $CdSe/TiO_2$,[17] Cu_2O/TiO_2,[18] Bi_2S_3/TiO_2,[19] which exhibited enhanced visible light reactivity. Compared with these semiconductors (CdS, Cu_2O, etc.), the motivation for using the perovskite oxides to couple with TiO_2 derives from their high chemical stability,[20] wide varieties and many oxides can be chosen to couple with TiO_2 because of narrower band gaps, as compared to that of TiO_2. Recently, hierarchically core-shell heterostructured photocatalysts, based on TiO_2 and perovskite oxides, such as $BiFeO_3/TiO_2$,[21] $BaTiO_3/TiO_2$,[22] $PbTiO_3/TiO_2$,[15] have been successfully synthesized. The composites offer a new and effective strategy for overcoming the barrier caused by the large band gap of TiO_2 and significantly enhancing the visible light photocatalytic efficiency.

The previous findings[15,23-24] suggest that in the heterostructured composites of TiO_2 and perovskite oxides, visible light is absorbed by the perovskite component, carriers generated in the perovskite and possibly separated by an internal field at the interface, and dye degradation occurred on the TiO_2 shell. Internal fields in composites can arise from ferroelectric polarization phenomena, p-n junctions and so on.[25] Therefore, considering the photogenerated charge carries separation and transfer of them from the perovskites to TiO_2, large-scale sharp interfaces with well-crystallization between the perovskite oxides and TiO_2 are highly desirable to enhance photocatalytic activity in visible light region.

In this work, we report a facile preparation of single-crystal heterostructured nanofiber composites $TiO_2/PbTiO_3$ consisting of TP-PTO nanofiber and anatase TiO_2 nanorods using a hydrothermal approach and, then, annealing at 650 ℃ where PP-PTO and TBOT were used as precursors. The scenario for the heterostructured nanofiber composites preparation is described in Fig. 1, and the preparation details are described in the Experimental Section. To the best of our knowledge, the one-dimensional (1D) ferroelectric nanocomposites, consisting of monocrystalline component phases, have not yet been realized. The heterostructured composites $TiO_2/PbTiO_3$ show greatly enhanced photocatalytic activity for degradation of MB, as compared to PTO and P25, under visible light irradiation.

Experimental details

Synthesis: Single-crystal PP-PTO nanofibers[26] were loaded with

TiO_2 nanorods using the hydrothermal method by the hydrolysis of TBOT as a Ti source. In detail, solutions were prepared by mixing different amounts of TBOT for 0.3mL, 0.4mL, 0.5mL, 0.7mL with 25mL of ethanol and stirring for 30 min. Next, 1.0 g of PP-PTO nanofibers were introduced into the obtained solutions and stirred for another 180 min to get homogeneous suspensions. 5.0 mL of $NH_3 \cdot H_2O$ was then added drop-wise into the suspensions as a mineralizer with stirring for 20min, and 5.0 mL of deionized water was added to promote the hydrolysis of TBOT and kept stirring for another 20 min. Thereafter, the suspensions were transferred to 50 mL Teflon-sealed autoclaves and maintained at 200 ℃ for 12 h under auto generated pressures. After natural cooling to room temperature, the resulting composites were collected, rinsed by ethanol for several times, and dried at 60 ℃ for 12 h. Finally, these composites were annealed in air to transform the single-crystal PP-PTO nanofibers into single-crystal TP-PTO nanofibers and crystallize the TiO_2 nanorods on the nanofibers. The composites were heated rapidly to 650 ℃, and annealed for 1 h at 650 ℃, and then naturally cooled to room temperature. As a comparison, single-crystal TP-PTO nanofibers were prepared using the same procedure but without the addition of TBOT. The diagrammatic sketch in Fig.1 represents the formation process of nanofiber composites.

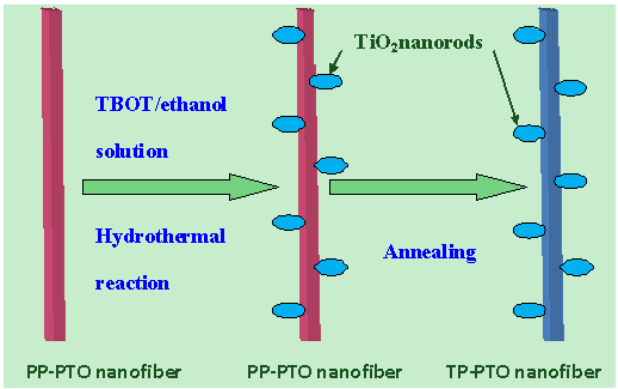

Fig.1 A proposed scheme for fabrication of the nanofiber composites consisting of TP-PTO nanofiber and TiO_2 nanorods.

Characterization: The crystal structures of the final products were characterized by means of X-ray diffraction on RIGAKUD-MAX-C with Cu Kα(λ=1.54056 Å) radiation, and the step size of 0.02° and scanning rate of 4°/min were used. SEM images were taken by a Hitachi field emission SEM MODEL S-4800. The structures and morphologies of the heterostructured composite were analyzed by transmission electron microscopy (TEM) and high-resolution TEM (HRTEM) on Tecnai G2 F20 using an accelerating voltage of 200 kV. The TEM sample was prepared by dispersing the powder ultrasonically in ethanol and then distributing a small drop of the suspension onto a copper micro grid. Diffuse reflectance spectroscopy (DRS) was employed to investigate the optical properties of samples on a UV-vis-NIR spectrophotometer (UV-3600, Shimadzu).

Photocatalytic experiments: The rate of photodegradation of MB under visible light irradiation was used to evaluate the photocatalytic activity of the powders based on the absorption spectroscopic technique. In a typical process, 0.1 g photocatalyst and 100 mL of the 1×10^{-5} M MB aqueous solution were mixed in a 100 mL quartz vessel. After reaching absorption/desorption equilibrium between the photocatalyst and the dye in the dark for 40 min, the vessel was exposed to the visible light produced by a 400 W Xenon lamp equipped with a UV cutoff filter (λ＞400 nm) under ambient conditions and stirring. After every given time interval, 5 mL of the photoreacted suspension was taken, centrifuged and analyzed by a UV-visible spectrophotometer (TU1901). The absorption peak at 664 nm was recorded, and the peak intensity was related to the MB photodegradation.

Results and discussion

3.1. Structure and morphology of the nanofiber composites. Fig.2 presents the XRD patterns of the single-crystal $TiO_2/PbTiO_3$ heterostructured nanofiber composites prepared by adding different amounts of TBOT. As shown in Fig.2, all the reflection peaks in these patterns can be readily indexed to perovskite TP-PTO (JPCDS 06-0452) and anatase TiO_2 (JCPDS 21-1272). It is revealed that the TP-PTO nanofibers are highly crystallized. No diffraction peaks corresponding to other impurities are detected indicating that the $TiO_2/PbTiO_3$ heterostructured nanofiber composites with a high purity have been fabricated by our experimental scheme.

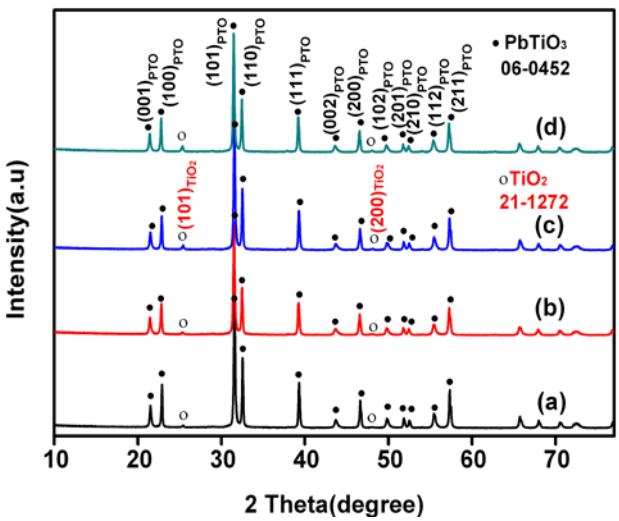

Fig.2 XRD patterns of (a) $TiO_2/PbTiO_3$ TBOT：0.3mL(the molar ratio of $TiO_2/PbTiO_3$ is 26.7%), (b) $TiO_2/PbTiO_3$ TBOT：0.4mL(the molar ratio of $TiO_2/PbTiO_3$ is 35.6%), (c) $TiO_2/PbTiO_3$ TBOT：0.5mL(the molar ratio of $TiO_2/PbTiO_3$ is 44.5%), (d) $TiO_2/PbTiO_3$ TBOT：0.7mL(the molar ratio of $TiO_2/PbTiO_3$ is 62.3%). The explanation after $TiO_2/PbTiO_3$ represents the addition amount of TBOT in the preparation of the composite.

SEM images of the nanofiber composites with 26.7%, 35.6%, 44.5% and 62.3% molar ratio of $TiO_2/PbTiO_3$ were prepared (Fig.3a-d). As shown in Fig.3a, the TiO_2 nanorods grow on the surface of the PTO nanofibers sparsely when the molar ratio of $TiO_2/PbTiO_3$ is 26.7%. As the molar ratio of $TiO_2/PbTiO_3$ is increased from 26.7% to 35.6%, distribution of the nanorods on the surface of the nanofibers become dense and relatively uniform although the TiO_2 aggregation could not be avoided (Fig.3b). With the increase of the molar ratio of $TiO_2/PbTiO_3$ from 35.6% to 44.5% and 62.3%, the nanorod aggregations significantly develop and can be observed even on the surface of the nanofibers (Fig.3c-d). The PTO nanofibers have the diameter of 200nm-500nm and length from few to tens of micrometers,

while the size of TiO_2 nanorods are about 30 nm in diameter and 50-100 nm in length.

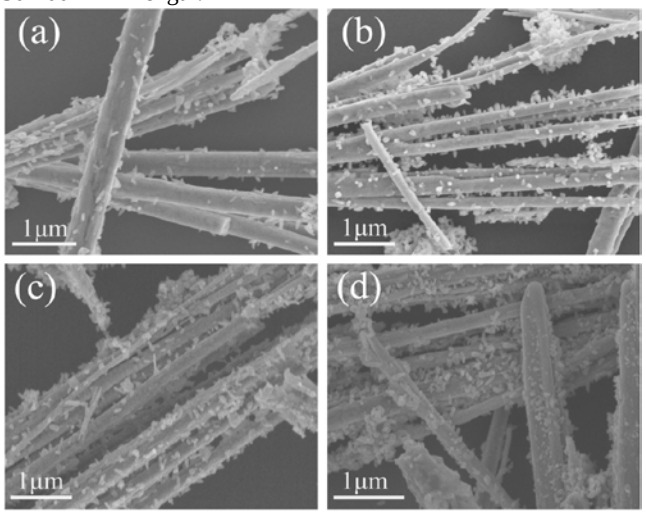

Fig.3 SEM images of (a) $TiO_2/PbTiO_3$ TBOT：0.3mL(the molar ratio of $TiO_2/PbTiO_3$ is 26.7%), (b) $TiO_2/PbTiO_3$ TBOT：0.4mL(the molar ratio of $TiO_2/PbTiO_3$ is 35.6%), (c) $TiO_2/PbTiO_3$ TBOT：0.5mL(the molar ratio of $TiO_2/PbTiO_3$ is 44.5%), (d) $TiO_2/PbTiO_3$ TBOT：0.7mL(the molar ratio of $TiO_2/PbTiO_3$ is 62.3%). The explanation after $TiO_2/PbTiO_3$ represents the addition amount of TBOT in the preparation of the composite.

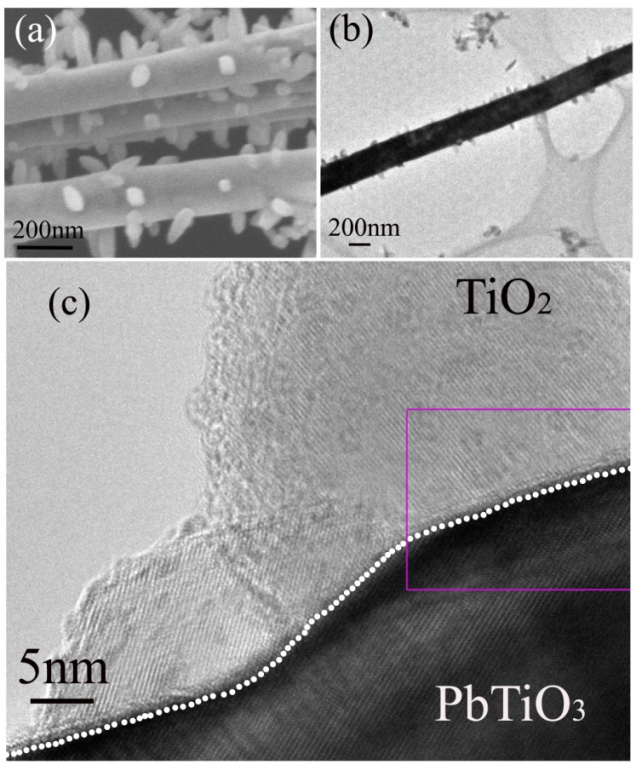

Fig.4 Microstructure analysis of the heterostructured nanofiber composites $TiO_2/PbTiO_3$ TBOT: 0.4mL(the molar ratio of $TiO_2/PbTiO_3$ is 35.6%): a typical SEM image (a) and TEM image (b) of the PTO nanofiber with dispersed TiO_2 nanorods on their surface, (c) HRTEM image of the heterostructured interface.

Fig.4a and b present typical SEM and TEM images of the heterostructured nanofiber composites $TiO_2/PbTiO_3$ TBOT: 0.4mL. As shown in Fig.4b, the single heterostructured nanofiber is composed of the PTO nanofiber (~ 300 nm in diameter) and TiO_2 nanorods (50~70 nm in length). The HRTEM image in Fig.4c shows clear and sharp interface with well-crystallization between the PTO nanofiber and the TiO_2 nanorods (the interface has been marked with the white dot line). To get further insight to the microstructure of the heterostructured interface, an enlarged HRTEM image caught from the area marked with a purple rectangle in Fig.4c is shown in Fig.5a. The 0.353 nm lattice fringe interval observed in Fig.5a agrees well with the (101) spacings of anatase TiO_2 (JCPDS 21-1272), and the observed lattice spacings in the PTO nanofiber are 0.391 nm and 0.284 nm, which can be indexed to the (100) and (011) crystal planes of perovskite TP-PTO (JPCDS 06-0452). As seen in Fig.5a, the difference between the interplanar distances of the planes (101) in anatase TiO_2 and (011) in perovskite PTO is large, and thus a disordered region of the width of 1-2 nm within the heterostructured interface is formed to reduce the growth barrier of the TiO_2 nanorods on the surface of the PTO nanofiber. The fast Fourier transformation (FFT) patterns (Fig.5b, c and d) corresponding to area 1, area 2 and the heterostructured interface area in Fig.5a, respectively, show sharp diffraction spots, indicating that the TiO_2 nanorods and the PTO nanofibers are well-developed single crystals in nature.

3.2. Optical and photocatalytic performance of the nanofiber composites. The optical absorption spectrum of semiconductor catalysts is critical to acquire their band gap and determine their photocatalytic performance. Fig.6 shows the absorption spectra of the samples transformed from the diffuse reflectance spectra (DRS) according to the Kubelka-Munk (K-M) method.[27] It is clear that there is almost no absorption for P25 when the wavelength of light is beyond 400 nm. In the case of PTO nanofibers, the absorption edge is about 2.63 eV and the value is lower than the previous results (2.75~3.60 eV) [28-31], possibly due to different morphology[32-33]. Such band gap of PTO nanofibers suggests a possibility of utilizing more visible light for photocatalysis. For sample $TiO_2/PbTiO_3$ TBOT: 0.4mL, the absorption edge is near 445 nm, corresponding to the band gap of 2.78 eV and indicating that the composites have absorption range extended to the visible-light spectrum, as compared to that of P25.

The photocatalytic activity of the heterostructured nanofiber composites for MB degradation are shown in Fig.7, and their reaction rates (Including PTO and P25), K_{MB}, which is represented as the slope of $\ln(C_0/C)$ vs time, are also shown in Table 1. As an organic heterocyclic-dye, MB is relatively stable under visible light if there is no catalyst added, and the degradation rate of MB is 0.00497min^{-1}, which is denoted as "blank" in Table 1. The PTO nanofibers demonstrate relatively high photocatalytic activity (0.00757 min^{-1}), compared to the P25 (0.00614 min^{-1}), which is mainly due to their smaller band gap. In stark contrast, remarkable degradation is achieved in the nanofiber composites as a photocatalyst. Especially, the composite $TiO_2/PbTiO_3$ TBOT: 0.4mL exhibits the highest activity, 0.02392 min^{-1}. About 90% of MB was decomposed after 100 min irradiation. When the content of TiO_2 exceeds 35.6 mol% (TBOT: 0.4mL), the photocatalytic activity of the nanofiber composites decreased owing to the excess amounts of TiO_2 in the composites, possibly shielding the visible-light absorption of PTO nanofibers from visible light irradiation. The composite $TiO_2/PbTiO_3$ TBOT: 0.4 mL demonstrated higher

photocatalytic activity compared to the heterostructured $PbTiO_3/TiO_2$[15] core-shell particles, which is very likely due to its shape interface and monocrystalline component phases.

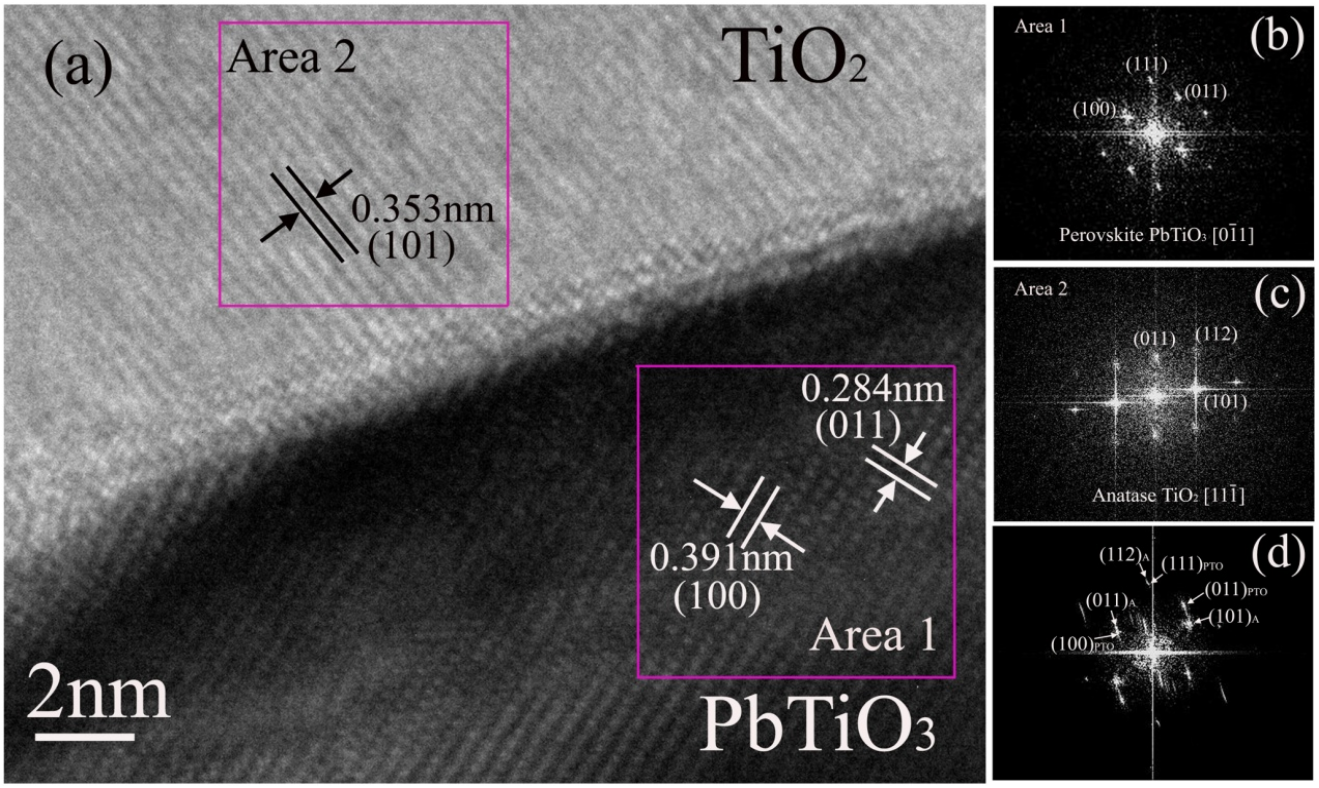

Fig.5 (a)An enlarged HRTEM image caught from the area marked with a purple rectangle in Fig.4c, fast Fourier transform (FFT) pattern corresponding to area 1 (b) and area 2 (c) in Fig.5a, (d) FFT pattern of the heterostructured interface area in Fig.5a.

Tab.1 Reaction rates of the heterostructured nanofiber composites, P25 and PTO for the photocatalytic degradation of MB (KMB).

	Blank	P25	PTO	$TiO_2/PbTiO_3$. TBOT:0.3mL	$TiO_2/PbTiO_3$ TBOT:0.4mL	$TiO_2/PbTiO_3$ TBOT:0.5mL	$TiO_2/PbTiO_3$ TBOT:0.7mL
K_{MB} (min^{-1})	0.00497	0.00614	0.00757	0.01216	0.02392	0.01052	0.00891

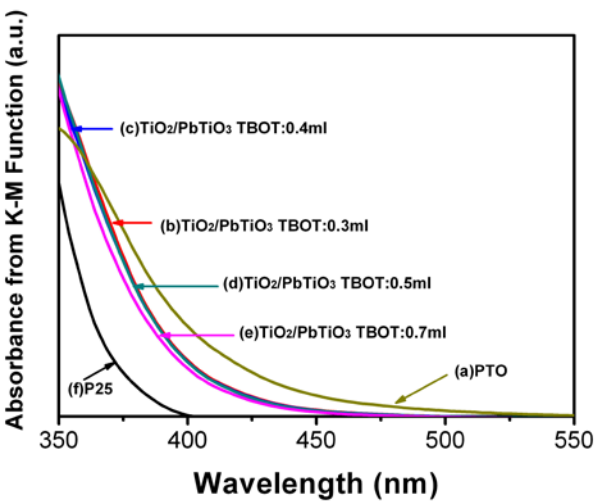

Fig.6 Absorbance data, converted from diffuse reflectance spectra (DRS) using Kubelka-Munk function. (a) PTO, (b) $TiO_2/PbTiO_3$ TBOT: 0.3mL, (c) $TiO_2/PbTiO_3$ TBOT: 0.4mL, (d) $TiO_2/PbTiO_3$ TBOT: 0.5mL, (e) $TiO_2/PbTiO_3$ TBOT: 0.7mL, (f) P25.

It has been proposed that carriers generated by the visible-light absorbing phase would be transferred to the TiO_2 surface, via the interface, to participate in dye degradation. The heterostructured nanofiber composites presented here have large-scale sharp crystalline interfaces, which are highly beneficial to the charge transfer and subsequent photocatalytic activity.

Furthermore, large-scale sharp interfaces with well-crystallization can promote charge separation and decrease the electron-hole recombination rate, by the aid of internal electric fields.[25] For example, it has been discussed that the internal bipolar field normal to the heterostructured interface, that arises from the spontaneous ferroelectric polarization, could lead to a band bending in the ferroelectric and, thus, separate photogenerated carriers,[15,22,34-36] such as the heteostructured $BaTiO_3/TiO_2$[22] and $PbTiO_3/TiO_2$[15] core-shell particles. In contrast, in our prepared nanofiber composites, the polarization orientation of TP-PTO nanofibers is parallel to the interfaces[37]. Therefore, such polarization can hardly contribute to the separation of charges across the interface. On the other hand, Kim et al.[38]

believed that the p-n diode formation in the $CaFe_2O_4/PbBi_2Nb_{1.9}W_{0.1}O_9$ composite was the reason that led to the high visible-light catalytic performance. Considering that $PbTiO_3$ is a p-type semiconductor[39-41] and TiO_2 is n-type[42-43], the possible formation of p-n junctions between the PTO and TiO_2 phase could result in the formation of space charge region and efficient separation of electron-hole pairs. The exact mechanism is not clear, and it will be explored in the future work.

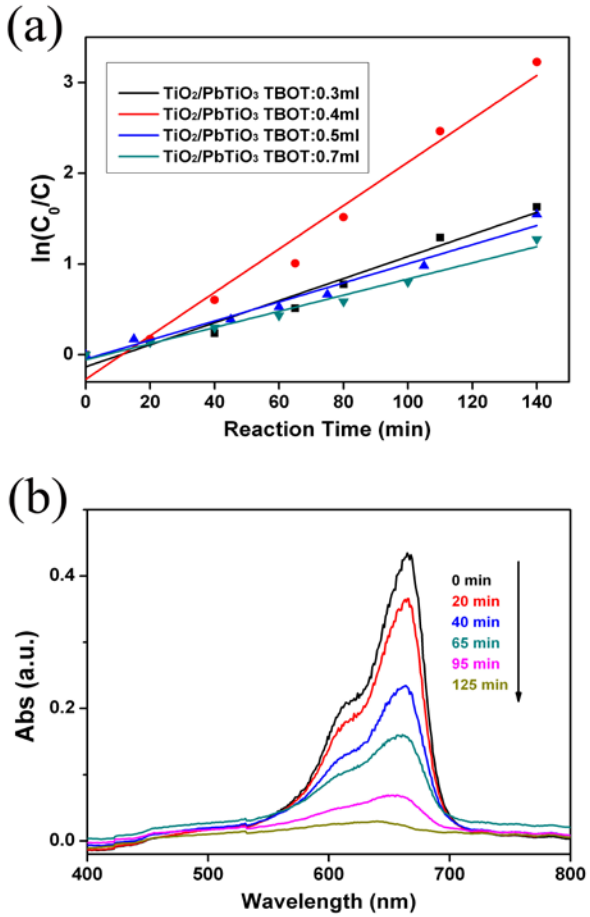

Fig.7 (a) Photodegradation of MB with the heterostructured nanofiber composites under visible light illumination; (b) Absorption changes of MB solution during photocatalytic process with the $TiO_2/PbTiO_3$ TBOT: 0.4mL under visible light illumination.

Conclusions

The single-crystal heterostructured nanofiber composite $TiO_2/PbTiO_3$ with novel configuration was designed and synthesized by a hydrothermal approach combined with annealing treatment at 650 ℃. Such heterostructured composites (especially $TiO_2/PbTiO_3$ TBOT: 0.4mL) demonstrate a high visible-light catalytic performance, which should be ascribed to its single-crystal component phases and shape interfaces, suggesting that this processing method could offer a possibility to acquire well-crystallization and sharp interfaces between perovskite oxides and titania.

Acknowledgement

This work was financially supported by the National Natural Science Foundation of China (No.51232006, 51102212 and 51102208) and Fundamental Research Funds for the Central Universities (No.2014FZA4009).

Notes and references

[a] *State Key Laboratory of Silicon Materials, Department of Materials Science and Engineering, Cyrus Tang Center for Sensor Materials and Application, Zhejiang University, Hangzhou, P.R. China*
[b] *Electron Microscope Center of Zhejiang University, Hangzhou, 310027, P.R. China*
**Corresponding author: E-mail: renzh@zju.edu.cn*
Tel: +86-571-87951649; Fax: +86-571-87952341
Email: hgr@zju.edu.cn
Tel:+86-571-87951649; Fax:+86-571-87952341

1 X.B. Chen, L.Liu, P.Y. Yu, S.S. Mao, *Science*, 2011, **331**, 746−750.
2 F. Han, V.S.R. Kambala, M. Srinivasan, D. Rajarathnam, R. Naidu, *Appl. Catal., A*, 2009, **359**, 25–40.
3 S. U. M. Khan, M. Al-Shahry, W. B. Ingler, *Science*, 2002, **297**, 2243-2245.
4 A.Fujishima, K. Honda, *Nature*, 1972, **238**, 37-38.
5 M.R. Hoffmann, S.T. Martin, W.Y. Choi, D.W. Bahnemannt, *Chem. Rev.*, 1995, **95**, 69.
6 J. Pascual, J. Camassel, H. Mathieu, Phys. Rev. B, 1978, **18**, 5606–5614.
7 H. Tang, F. Levy, H. Berger, P.E. Schmid, *Phys. Rev. B*, 1995, **52**, 7771–7774.
8 K. Nagaveni, M.S. Hegde, G. Madras, *J. Phys. Chem. B*, 2004, **108**, 20204-20212.
9 R. Asahi, T. Morikawa, T. Ohwaki, K. Aoki, Y. Taga, *Science*, 2001, **293**, 269-271.
10 J. Choi, H. Park, M.R. Hoffmann, *J. Phys. Chem. C*, 2010, **114**, 783-792.
11 H. Xu, L.Z. Zhang, *J. Phys. Chem. C*, 2010, **114**, 940-946.
12 Y.H Hu, *Angew. Chem. Int. Ed.*, 2012, **51**, 12410-12412.
13 W.K. Ho, J.C. Yu, J. Lin, J.G. Yu, P.S. Li, *Langmuir*, 2004, **20**, 5865-5869.
14 X. Zhang, L. Zhang, T. Xie, D. Wang, *J. Phys. Chem. C*, 2009, **113**, 7371−7378.
15 L. Li, Y. Zhang, A.M.Schultz, X.Liu, P.A. Salvador, G.S.Rohrer, *Catal. Sci. Technol.*, 2012, **2**, 1945−1952.
16 S.Q. Liu, N. Zhang, Z.R. Tang, Y.J. Xu, *ACS Appl. Mater. Interfaces*, 2012, **4**, 6378-6385.
17 S.C. Lo, C.F. Lin, C.H. Wu, P.H. Hsieh, J. Hazard. *Mater.*, 2004, **114**, 183-190.
18 L. Huang, F. Peng, H.J. Wang, H. Yu, Z. Li, *Catal. Commun.*, 2009, **10**, 1839-1843.
19 Y. Bessekhouad, D. Robert, J. Weber, *J. Photochem. Photobiol. A: Chem.*, 2004, **163**, 569-580.
20 I. Shakir, M. Shahid, D.J. Kang, *Chem. Eng. J.*, 2013, **225**, 650-655.
21 S. Li, Y.H. Lin, B.P. Zhang, J.F. Li, C.W. Nan, *J. Appl. Phys.*, 2009, **105**, 054310.
22 L. Li, G.S. Rohrer, P.A. Salvador, *J. Am. Ceram. Soc.*, 2012, **95**, 1414-1420.
23 Y.L. Zhang, A.M. Schultz, P.A. Salvador, G.S.Rohrer, *J. Mater. Chem.*, 2011, **21**, 4168–4174.
24 L. Li, X. Liu, Y.L. Zhang, N.T. Nuhfer, K. Barmak, P.A. Salvador, G.S. Rohrer, *ACS Appl. Mater. Interfaces*, 2013, **5**, 5064-5071.
25 L. Li, P.A. Salvador, G.S. Rohrer, *Nanoscale*, 2014, **6**, 24-42.
26 Z.H. Ren, G. Xu, Y. Liu, X. Wei, Y.H.Zhu, X.B. Zhang, G. Lv, Y.W. Wang, Y.W. Zeng, P.Y. Du, W.J. Weng, G. Shen, J.Z. Jiang, G.R. Han, *J. Am. Chem. Soc.*,2010, **132**, 5572-5573.
27 P. Kubelka, F. Munk, Z. Tech. Phys., 1931, **12**, 593-601.
28 D. Arney, T. Watkins, P.A. Maggard, *J. Am. Ceram. Soc.*, 2011, **94**, 1483–1489.
29 V.I. Zametin, *Phys. Status Solidi B*, 1984, **124**, 625–640.
30 S.M. Hosseini, T. Movlarooy, A. Kompany, *Phys. B*, 2007, **391**, 316–321.
31 H.O.Yadav, *Ceram. Int.*, 2004, **30**, 1493–1498.
32 B.B. Kale, J.O. Baeg, S.M. Lee, H. Chang, S.J. Moon, C.W. Lee, *Adv. Funct. Mater.*, 2006, **16**, 1349-1354.

33 A.P. Alivisatos, **Science**, 1996, **271**, 933-937.
34 P.S. Brody, *Solid State Commun*, 1973, **12**, 673-676.
35 P.S. Brody, *J. Solid State Chem.*, 1975, **12**, 193-200.
36 V.M. Fridkin, *Ferroelectrics*, 1984, **53**, 169-187.
37 Z.Y.Liu, Z.H.Ren, Z. Xiao, C.Y. Chao, X. Wei, Y. Liu, X. Li, G. Xu, G. Shen, G.R. Han, *Small*, 2012, **8**, 2959-2963.
38 H.G. Kim, P.H. Borse, W.Y. Choi, J. S. Lee, *Angew. Chem. Int. Ed.*, 2005, **44**, 4585-4589.
39 P.W.M. Blom, R.M. Wolf, J.F.M. Cillessen, M.P.C.M. Krijn, *Phys. Rev. Lett.*, 1994, **73**(15), 2107-2110.
40 Z. Zhang, P. Wu, L. Lu, C. Shu, *Appl. Phys. Lett.*, 2006, **88**, 142902.
41 I. Popescu, I. Săndulescu, Á. Rédey, I.-C. Marcu, *Catal. Lett.*, 2011, **141**, 445-451.
42 P. Kofstad, *New York: Wiley*, 1972.
43 M.K. Nowotny, P. Bogdanoff, T. Dittrich, S. Fiechter, A. Fujishima, H. Tributsch, *Mater. Lett.*, 2010, **64**, 928-930.

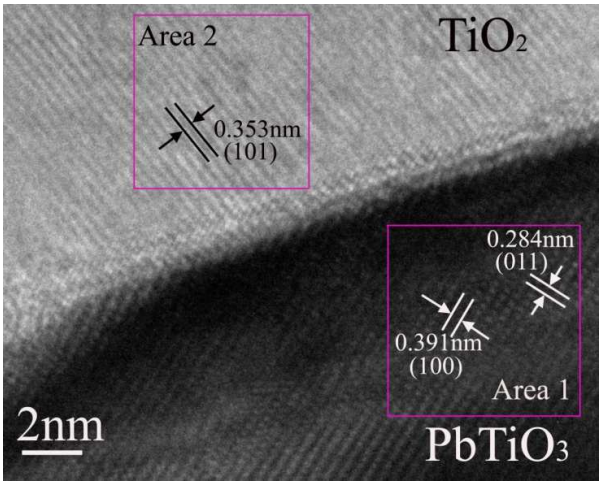

For single-crystal $TiO_2/PbTiO_3$ nanofiber composites, anatase TiO_2 nanorods grew on the surface of tetragonal perovskite (TP) $PbTiO_3$ nanofibers and form sharp $TiO_2/PbTiO_3$ interfaces, leading to single-crystal heterostructures, which were highly beneficial for charge transfer and separation between two phases.